IEEE Access
Multidisciplinary | Rapid Review | Open Access Journal

Received September 3, 2016, accepted September 16, 2016, date of publication September 21, 2016,
date of current version October 6, 2016.

Digital Object Identifier 10.1109/ACCESS.2016.2611530

Fractal Dimension Estimation for Developing Pathological Brain Detection System Based on Minkowski–Bouligand Method

YU-DONG ZHANG[1,10], XIAN-QING CHEN[2], TIAN-MING ZHAN[3], ZHU-QING JIAO[4], YI SUN[5], ZHI-MIN CHEN[6], YU YAO[7], LAN-TING FANG[8], YI-DING LV[9], AND SHUI-HUA WANG[1]

[1]School of Computer Science and Technology, Nanjing Normal University, Nanjing 210023, China
[2]Department of Electrical Engineering, College of Engineering, Zhejiang Normal University, Jinhua 321004, China
[3]School of Technology, Nanjing Audit University, Nanjing 211815, China
[4]School of Information Science and Engineering, Changzhou University, Changzhou 213164, China
[5]State Key Laboratory of Networking and Switching Technology, Beijing University of Posts and Telecommunications, Beijing 100876, China
[6]School of Electronic Information, Shanghai Dianji University, Shanghai 200240, China
[7]School of Information Engineering, Huadong Jiaotong University, Nanchang 330013, China
[8]School of Information Science and Engineering, Southeast University, Nanjing 210096, China
[9]Department of Psychiatry, Nanjing Medical University, Nanjing 210029, China
[10]Hunan Provincial Key Laboratory of Network Investigational Technology, Hunan Policy Academy, Changsha 410138, China

Corresponding author: S.-H. Wang (wangshuihua@njnu.edu.cn)

This work was supported in part by the NSFC under Grant 61602250 and Grant 61502206, in part by the Natural Science Foundation of Jiangsu Province under Grant BK20150983 and Grant BK20150523, in part by the Open Research Fund of Hunan Provincial Key Laboratory of Network Investigational Technology under Grant 2016WLZC013, and in part by the Open Fund of Fujian Provincial Key Laboratory of Data Intensive Computing under Grant BD201607.

ABSTRACT It is of enormous significance to detect abnormal brains automatically. This paper develops an efficient pathological brain detection system based on the artificial intelligence method. We first extract brain edges by a Canny edge detector. Next, we estimated the fractal dimension using box counting method with grid sizes of 1, 2, 4, 8, and 16, respectively. Afterward, we employed the single-hidden layer feedforward neural network. Finally, we proposed an improved particle swarm optimization based on three-segment particle representation, time-varying acceleration coefficient, and chaos theory. This three-segment particle representation encodes the weights, biases, and number of hidden neuron. The statistical analysis showed the proposed method achieves the detection accuracies of 100%, 98.19%, and 98.08% over three benchmark data sets. Our method costs merely 0.1984 s to predict one image. Our performance is superior to the 11 state-of-the-art approaches.

INDEX TERMS Minkowski Bouligand dimension, genetic algorithm, artificial bee colony, logistic map, number of hidden neuron, K-fold cross validation.

I. INTRODUCTION

Pathological brain detection system (PBDS) can help neuroradiologists to detect specific disease for patients. There are massive of neuroimaging methods [1], such as CT, PET, SPECT, and MRI. The MRI is radiation free [2] and can provide better resolution in brain soft tissues [3]; thus, we chose MRI as the main scanning tool for the brain image.

There are two techniques to develop preliminary PBDS: (i) based on single slice [4] and (ii) based on the whole brain [5]. The former is inexpensive and rapid for scanning, but it needs to select the slice including the lesion. The latter is time-consuming, and needs complexed algorithms. In this study, we center in the former one.

In the last decade, numerous PBDSs are developed. Hachaj and Ogiela [6] applied self-organizing map (SOM) to detect perfusion regions in abnormal brains. El-Dahshan et al. [7] employed the feedback pulse-coupled neural network (PCNN) to preprocess the brain images. Then they combined discrete wavelet transform (DWT) and PCA to extract features. They finally employed back propagation neural network (BPNN). Feng [8] employed stationary wavelet transform (abbreviated as SWT) to take place of traditional DWT. Afterwards, to train the classifier, they introduced a novel algorithm that is a hybridization of PSO and ABC (shorted as HPA). Sun [9] combined Hu moment invariants (HMI) with wavelet entropy. They used generalized eigenvalue proximal SVM (GEPSVM). Wibmer et al. [10] proposed a novel

Haralick texture as image feature. Dong et al. [11] proposed a new image feature as wavelet packet Tsallis entropy (WPTE) and wavelet packet Shannon entropy (WPSE). They proved WPTE is the extension of WPSE, i.e., WPSE is a particular case of WPTE. In this study, we employed WPTE to extract features. Dong et al. [12] used stationary wavelet transform (SWT) and PCA.

We aimed to develop a novel PBDS from a different viewpoint. In fractal geometry, the fractal dimension (FD) is a measure to provide how fractal pattern changes within the scale where it was measured. What is more, the FD is already proven to be an effective measure for brain morphometry. Rajagopalan et al. [13] observed brain white matter changes in amyotrophic lateral sclerosis (ALS) from FD study. Farahibozorg et al. [14] observed age- and sex-related difference in the complexity of the global and hemispheric white matter (WM) through FD. Therefore, it is reasonable to extend to extract features from the pathological brain images via FD.

On the other hand, single-hidden layer feedforward neural-network (SLFN) is commonly used as a classifier, since it can approximate functions with desired accuracy. However, training performance of SLFN influences the classification accuracy. At present, many swarm intelligence based methods have proven excellent results. Mirjalili et al. [15] proposed to use social spider algorithm (SSA). Gholizadeh [16] used a modified firefly algorithm (MFA). Lahmiri [17] applied particle swarm optimization (PSO). Those methods can achieve good results, but they may be trapped into local minima and their convergence speed is a bit slow.

To further improve the training efficiency, we proposed an improved PSO. The remainder of this paper is organized as follows: Section II provides the materials. Section III introduces the fractal dimension estimation. Section IV introduces the basic fundamentals of SLFN. Section V proposes an improved PSO algorithm. Section VI gives the implementation pseudocodes. Section VII offers the experimental results and discussions. Section VIII concludes the paper.

II. MATERIALS AND STATISTICAL ANALYSIS

Three open access dataset were commonly used in PBD systems comparison. The slices were selected by neuroradiologists with experiences over ten years. They are of different slices of brain magnetic resonance (MR) images. The first dataset (D_1) contains 66 brain images, the second dataset (D_2) contains 160 images, and the third dataset (D_3) contains 255 images. Their descriptions can be found in reference [18].

The brain images from the three datasets are all T2-weighted and have a size of 256×256. Several samples of pathological brains were illustrated in Figure 1. We did not use the brain extraction tool (BET) to remove the skulls, since some diseases may involve the meninges, such as subarachnoid stroke. Therefore, our PBDS can detect deforms in skulls compared to traditional PBDS.

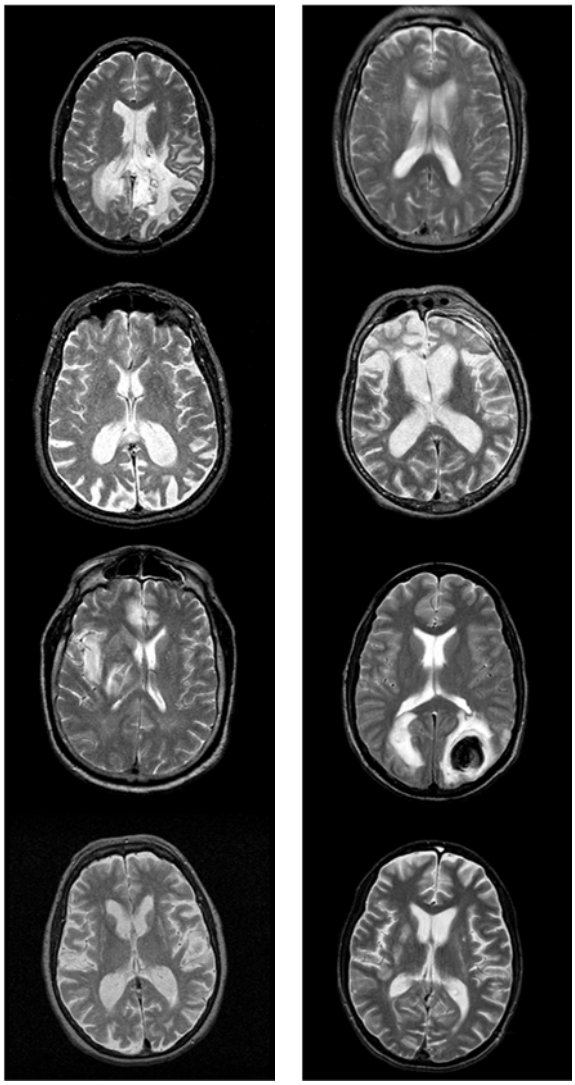

FIGURE 1. Sample of pathological brains.

Besides, we did not center the brain in the image, since it is also unnecessary for recent advanced face recognition methods to center the faces.

The stratified cross validation (SCV) was used [19]. Following common convention and the stratification, a 6-fold SCV was employed for D_1, and a 5-fold SCV was employed for D_2 and D_3. In this way, each fold can get similar class distribution. Table 1 presents the statistical setting of three datasets.

TABLE 1. Statistical setting.

Dataset	F.N.	R.N.	T		V	
D_1	6	10	H (15)	P (40)	H (3)	P (8)
D_2	5	10	H (16)	P (112)	H (4)	P (28)
D_3	5	10	H (28)	P (176)	H (7)	P (44)

(H = Healthy; P = Pathological; T = Training; V = Validation; R.N. = Run Number; F.N. = Fold Number.)

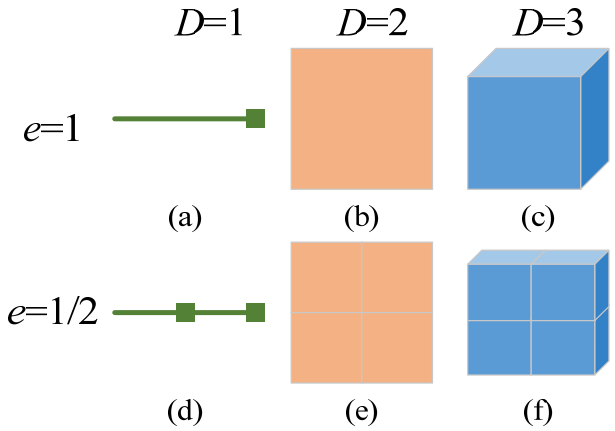

FIGURE 2. Relationship among scaling and dimension: (a) $N = 1$; (b) $N = 1$; (c) $N = 1$; (d) $N = 2$; (e) $N = 4$; (f) $N = 8$. In the figure, e represents the scaling factor, D the fractal dimension.

III. FRACTAL DIMENSION ESTIMATION

A. MODEL

In the field of fractal geometry, the fractal dimension (FD) [20] offers a statistical index of complexity, measuring the pattern detail changes with the scale [21]. We will try to use simple illustrations to show the concept of FD. Suppose N represents the number of sticks for measuring, e the scaling factor, D the fractal dimension, then we have Figure 2, and then can summarize as

$$N = \left(\frac{1}{e}\right)^D \tag{1}$$

This scaling rule validates conventional observations about geometry and dimension. Then, equation (1) can be extended to fractal field by the simple transformation as

$$D = -\log_e N \tag{2}$$

For example, the Koch curve [22] is generated by dividing a line segment into three equal-length segments, drawing an equilateral triangle over the middle segment as its base, and removing the base. The Koch curve has an $N = 4$ when $e = 1/3$, thus its fractal dimension is $D = 1.2619$. Figure 3 shows the one to four iterations of Koch curve, generated by our developed computer programs.

B. BRAIN EDGE DETECTION

Image preprocessing is necessary, since the fractal dimension works better for binary image than grayscale image. Lahmiri and Boukadoum [23] proposed an edge fractal dimension, and spectral energy signature. Du et al. [24] generated leaf edge using multiple threshold technique, and utilized fractal dimension feature to recognize plant leaf. Yarlagadda et al. [25] used the fractal dimension value of facial edge to classify subjects to different age groups. Amarasinghe et al. [26] employed edge detection algorithm to obtain fractal dimension of long electrical discharge. Zhong et al. [27] used edge detection technique in CT images.

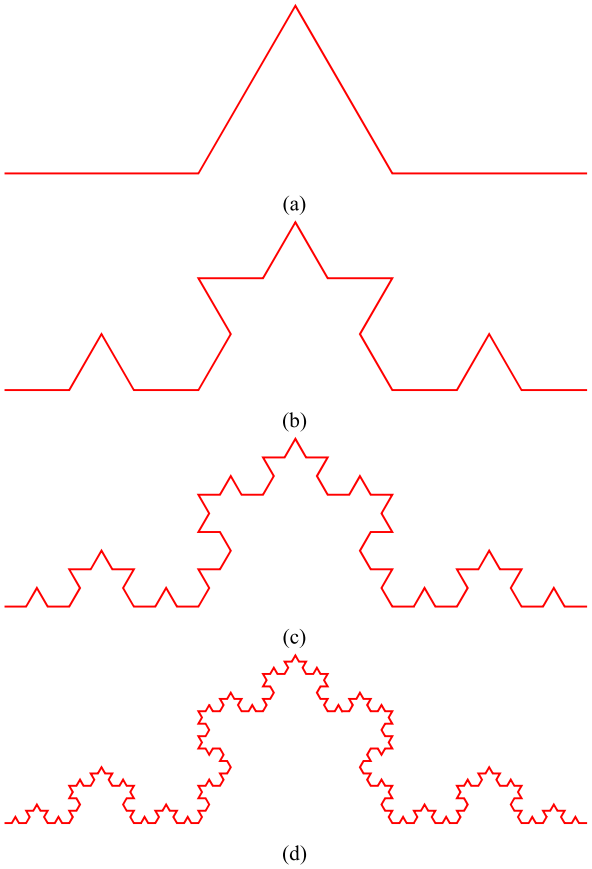

FIGURE 3. Koch curve: (a) one iteration; (b) two iterations; (c) three iterations; (d) four iterations.

From above methods, we see that edge detection is an effective preprocessing method for fractal dimension calculation. It can transform the natural image to binary image, and meanwhile it can preserve the key features. In this study, we shall test fiver different edge detection algorithms: Laplacian of Gaussian (LOG), Prewitt, Roberts, Sobel, and Canny.

The edge detection may incur spurious points on the edge, hence, the "edge thinning" [28] technique is necessary to remove them. In ideal condition, it can provide one-pixel thick edge. Besides, thin edges can give better efficiency in object detection [29].

C. MINKOWSKI-BOULIGAND DIMENSION

Minkowski-Bouligand dimension (MBD) [30], is a way of estimating the fractal dimension, by imaging the pattern lying over an equally-spaced grid and counting how many boxes are required to cover [31]. The box counting method can get the curve of required boxes with the grid scale [32]. This curves are the brain edges in our study.

Figure 4 shows an illustration of using box counting method to calculating the required box at grid size of 64, 32, and 16, respectively. The results showed that the required box numbers are 11, 37, and 116, respectively. Therefore, the required box numbers are chosen as the image features, which reflects the fractal dimension at different grid size.

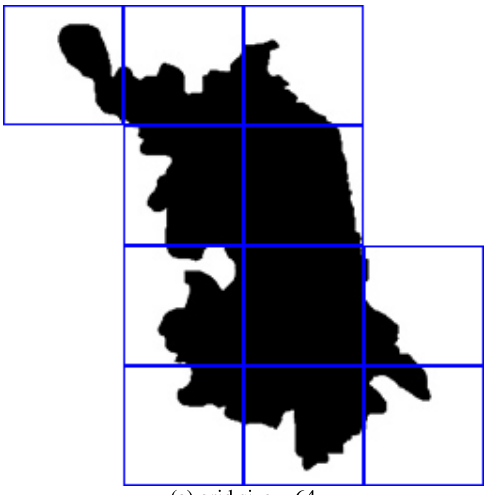
(a) grid size = 64

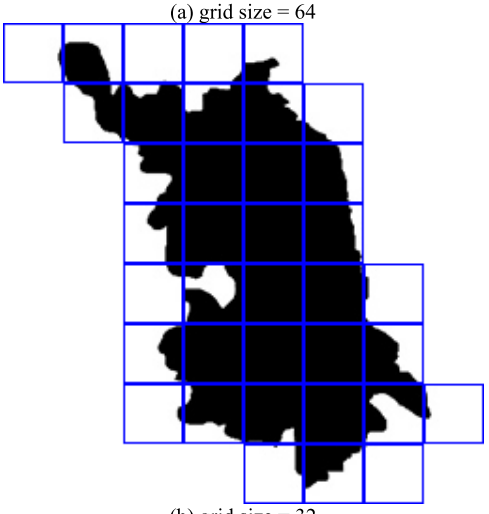
(b) grid size = 32

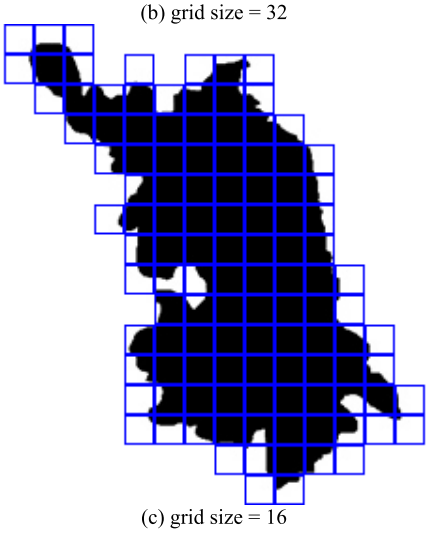
(c) grid size = 16

FIGURE 4. box counting algorithm on the Jiangsu map with size of 256×256.

IV. SINGLE-HIDDEN LAYER FEEDFORWARD NEURAL-NETWORK

The single-hidden layer feedforward neural-network (SLFN) maps input feature to target class [33], by constructing a fully connected [34] feedforward neural network with only one hidden layer [35]. It is reported to have better performances than decision tree and support vector machine. Figure 5 gives the structure of SLFN pictorially.

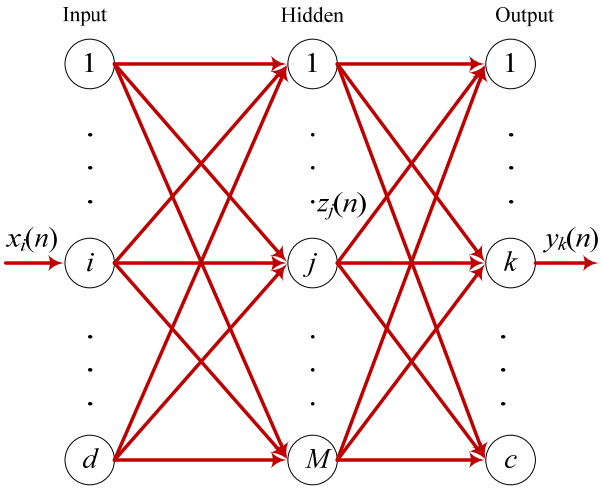

FIGURE 5. Structure of SLFN (*x* represents the input data, *y* the output data, *n* the index of sample, *d* the number of input neurons, *M* the number of hidden neurons, *c* the number of output neurons, *i* the index of input neuron, *j* the index of hidden neuron, *k* the index of output neuron).

Suppose $[\mathbf{x}(n), \mathbf{t}(n)]$, $(n = 1, 2, \ldots, N)$ denotes the n-th training data, we have:

$$\mathbf{x}(n) = [x_1(n), x_2(n), \ldots, x_d(n)]^T \quad (3)$$

$$\mathbf{t}(n) = [t_1(n), t_2(n), \ldots, t_c(n)]^T \quad (4)$$

where d represents the dimension of input features, c the number of classes, and $()^T$ the transpose operator. The training of SLFN will generate realistic output $\mathbf{y}(n)$ as

$$\mathbf{y}(n) = [y_1(n), y_2(n), \ldots, y_c(n)]^T \quad (5)$$

All training algorithms are to minimize the sum of mean-squared error (MSE) between the target vector $\mathbf{t}(n)$ and realistic output vector $\mathbf{y}(n)$ as

$$\min \sum_{n=1}^{N} (\mathbf{y}(n) - \mathbf{t}(n))^2 = \min \sum_{n=1}^{N} \sum_{k=1}^{c} (y_k(n) - t_k(n))^2 \quad (6)$$

For each neuron in hidden layer and output layer, the model is depicted in Figure 6. The inputs are weighted by multiplying with weights $\mathbf{w}$, and the results are added with a

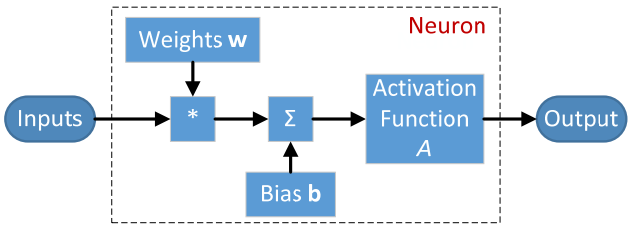

FIGURE 6. Structure of a neuron.

bias matrix **b**. After the summed results are passed through an activation function A, the final output is generated.

V. OPTIMIZATION

In the last decade, swarm intelligence methods were employed to train the SLFN. For instance, Hu et al. [36] used genetic algorithm (GA). Han and Zhu [37] employed the particle swarm optimization (PSO). Hassim and Ghazali [38] used artificial bee colony (ABC) algorithm. Yang et al. [39] utilized the biogeography-based optimization (BBO).

Those algorithms achieve better results than traditional gradient-descent related algorithms, since the optimization is ill-conditioning and contains many local minimal points. Nevertheless, they still suffer from following other aspects: (i) The training algorithms are not robust; and (ii) They can only optimize the weights, but cannot optimize the number of hidden neuron (NHN) in the same time.

A. THEORY OF PSO

In this study, we chose PSO .[40] as the main algorithm and proposed three improvements. In canonical PSO, each particle represents a candidate solution. Both the position P and the velocity V are associated with each particle. "Velocity clamping" [41] was used to limit particles flying out of the search space.

The fitness function f is evaluated for all the particles at each iteration. Then, two kinds of best particles are selected. One is the previous best (b_p) position a particle has traversed so far [42], with definition as

$$b_p(i,t) = \arg\min_{k=1,\ldots,t} [f(P_i(k))] \tag{7}$$

where f the fitness function, N the total number of particles, i denotes the particle index, k the iteration index, t the current iteration number, $P_i(k)$ the position of i-th particle at k-th iteration. The other is the global best (b_g) position that all particles have traversed so far [43], defined as

$$b_g(t) = \arg\min_{i=1,\ldots,N} \left[b_p(i,t)\right] \tag{8}$$

Hence, the two properties of every particle are updated as follows

$$\begin{aligned} V_i(t+1) = {} & \omega V_i(t) \\ & + r_p c_p \left(b_p(i,t) - P_i(t)\right) + r_g c_g \left(b_g(t) - P_i(t)\right) \end{aligned} \tag{9}$$

$$P_i(t+1) = P_i(t) + V_i(t+1) \tag{10}$$

Here ω represents the inertia weight, with purpose to balance the global exploration and local exploitation [44]. r_p and r_g are uniformly distributed random variables within range [0, 1]. Two positive constant parameters c_p and c_g are called "acceleration coefficients" to modify the distance towards previous best and global best, respectively [45].

B. PROPOSED IMPROVED PSO

To further enhance the performance of PSO and to solve the three shortcomings of swarm intelligence in classifier training, we thus propose an improved PSO method in this paper based on a novel representation method, the time-varying acceleration coefficient (TVAC) strategy, and chaos theory.

A three-segment particle representation (TSPR) was proposed, which divides the particle into three segments. Figure 7 shows that the first segment was encoded as the weights of SLFN, the second segment was encoded as the bias, and the third segment as the number of hidden neurons (NHN).

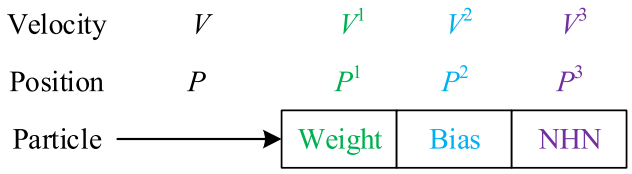

FIGURE 7. Technique of three-segment particle representation. (NHN represents the number of hidden neurons).

From Figure 7 and Figure 8, the position $P_i(t)$ and velocity $V_i(t)$ of i-th particle at t-th iteration can be rewritten as

$$P_i(t) = \left[\, P_i^1(t) \quad P_i^2(t) \quad P_i^3(t) \,\right] \tag{11}$$

$$V_i(t) = \left[\, V_i^1(t) \quad V_i^2(t) \quad V_i^3(t) \,\right] \tag{12}$$

Accordingly, the previous best b_p of i-th particle at t-th iteration can be expressed as

$$b_p(i,t) \triangleq \left[\, b_p^1(i,t) \quad b_p^2(i,t) \quad b_p^3(i,t) \,\right] \tag{13}$$

and the global best b_g at t-th iteration can be expressed as

$$b_g(t) = \left[\, b_g^1(t) \quad b_g^2(t) \quad b_g^3(t) \,\right] \tag{14}$$

Based on above definitions, the update rules (9)(10) should be adjusted to be coherent with the TSPR as

$$V_i(t+1) = \left[\, V_i^1(t+1) \quad V_i^2(t+1) \quad V_i^3(t+1) \,\right] \tag{15}$$

The three segments of $V_i(t+1)$ are defined as

$$\begin{aligned} V_i^1(t+1) = {} & \omega_1 V_i^1(t) \\ & + d_{p,1}(t) c_p(t) \left(b_p^1(i,t) - P_i^1(t)\right) \\ & + d_{g,1}(t) c_g(t) \left(b_g^1(t) - P_i^1(t)\right) \end{aligned} \tag{16}$$

$$\begin{aligned} V_i^2(t+1) = {} & \omega_2 V_i^2(t) \\ & + d_{p,2}(t) c_p(t) \left(b_p^2(i,t) - P_i^2(t)\right) \\ & + d_{g,2}(t) c_g(t) \left(b_g^2(t) - P_i^2(t)\right) \end{aligned} \tag{17}$$

$$\begin{aligned} V_i^3(t+1) = {} & \omega_3 V_i^2(t) \\ & + d_{p,3}(t) c_p(t) \left(b_p^3(i,t) - P_i^3(t)\right) \\ & + d_{g,3}(t) c_g(t) \left(b_g^3(t) - P_i^3(t)\right) \end{aligned} \tag{18}$$

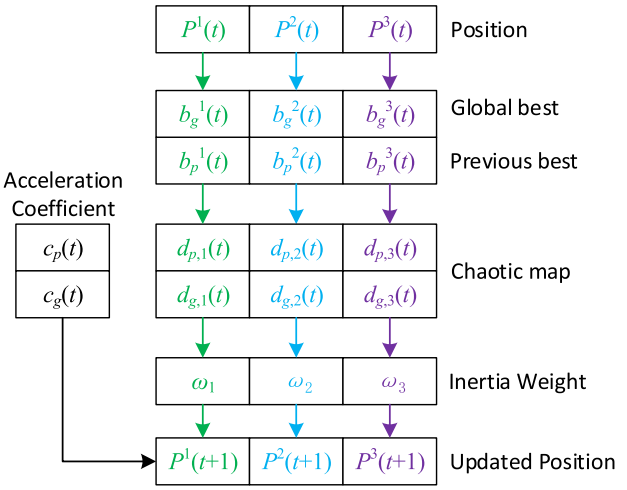

FIGURE 8. New Update Rules.

where the other two improves are also imbedded: On one hand, the two factors c_p and c_g are modified as adaptive based on the time-varying acceleration coefficient (TVAC) [46] strategy as

$$c_p(t) = (c_{p,f} - c_{p,i}) \times \frac{t}{t_f} + c_{p,i} \tag{19}$$

$$c_g(t) = (c_{g,f} - c_{g,i}) \times \frac{t}{t_f} + c_{g,i} \tag{20}$$

where t_f was a predefined maximum iteration number. $c_{p,i}$ and $c_{p,f}$ are initial and final values of c_p. The same setting was applied to c_g. TVAC can enhance the global search ability in the initial stage, and augment the local search ability in the end stage [47]. In common, TVAC offers more weight on cognitive component in the initial, and more weight on social component in the end [48].

On the other hand, the two random variable r_p and r_g were replaced by six chaotic map series $d_{p,1}(t)$, $d_{p,2}(t)$, $d_{p,3}(t)$, $d_{p,4}(t)$, $d_{p,5}(t)$, $d_{p,6}(t)$. The chaos theory features in the butterfly effect [49], and it can bring more versatility into the population. The famous logistic map is employed, which is also a discrete time demographic model analogous to the logistic equation [50]. The model is written as:

$$d(t+1) = r \times d(t) \times [1 - d(t)] \tag{21}$$

where r represents the logistic parameter [51]. This equation will produce a chaotic series when r equals to 4 [52]. In all, we name this proposed method by particle swarm optimization with TSPR, TVAC, and chaos (PSO-TTC).

VI. IMPLEMENTATION

This proposed PBDS used MBD as features, used SLFN as classifiers, and proposed a novel PSO-TTC algorithm for optimization. The optimal parameters in PSO-TTC were obtained by grid-searching algorithm. Figure 9 lists the diagram of this proposed PBDS. Here we implement our method by following steps shown in Algorithm 1.

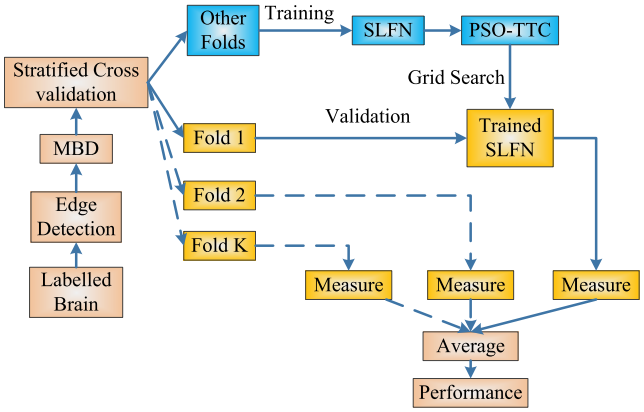

FIGURE 9. Diagram of this proposed PBDS (This will be repeated ten times).

Algorithm 1 Our proposed MBD + SLFN + PSO-TTC algorithm

Step 1: Extract edges from every labelled brain image;
Step 2: Extract MBD features from brain images with box sizes of 1, 2, 4, 8, and 16;
Step 3: Use stratified cross validation to divide the datasets into K-folds at random;
Step 4: Fold i was used for validation, and the other folds for training:
    Step 4.1: $i = 1, 2, 3, \ldots, K$;
    Step 4.2: The learning model was SLFN trained by PSO-TTC. Parameters were obtained by grid search;
    Step 4.3: The measure was recorded on the validation set of fold i;
Step 5: We average the measures and output the final performance.
Step 6: We repeat from Step 2 to Step 4 ten times, and output the averaged performance.

VII. RESULTS AND DISCUSSIONS

A. EDGE DETECTION

Figure 10(a) shows an original brain image, which indicates the patient suffers from metastatic adenocarcinoma. Figure 10(b-f) shows the edge detection result via five different techniques: LOG, Prewitt, Roberts, Sobel, and Canny. Those edge detectors are built-in functions in the Matlab software.

The comparison shows Canny algorithm can extract edge more efficiently while not removing important textures. The results in Figure 10 fall in line with other researches: Di and Gao [53] found Canny algorithm is the most suitable for 3D seismic discontinuity enhancement. Singh and Datar [54] showed Canny algorithm performed the best for secure color image steganography. Yasmin and Sathik [55] proved Canny algorithm give better performance in skin lesion border detector than other algorithms. All those confirmed the effectiveness of Canny algorithm.

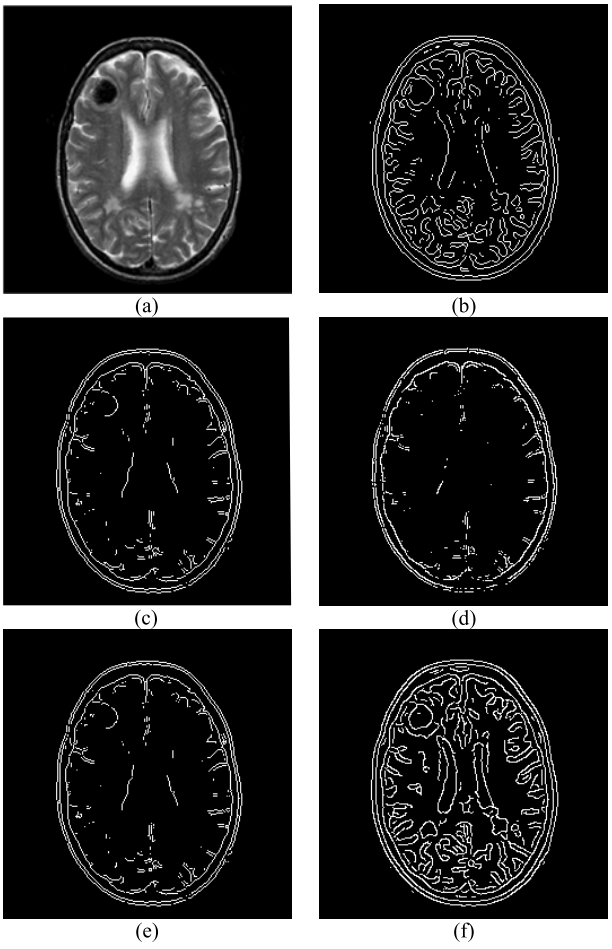

FIGURE 10. Comparison of brain edge detection. (a) Original Image. (b) LOG. (c) Prewitt. (d) Roberts. (e) Sobel. (f) Canny.

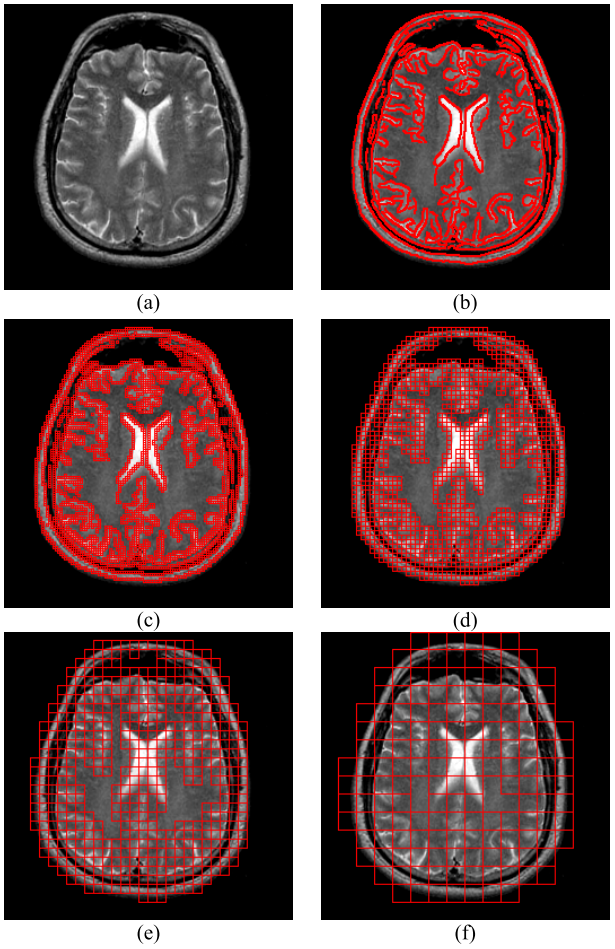

FIGURE 11. Fractal dimension estimation of brain MR images. (a) Original image. (b) grid size = 1. (c) grid size = 2. (d) grid size = 4. (e) grid size = 8. (f) grid size = 16.

B. FRACTAL DIMENSION OF BRAIN IMAGE

Next, Minkowski-Bouligand dimension (MBD) method was used to estimate the fractal dimension of brain images. Figure 11 shows the required boxes for this brain image is 5619, 3028, 1436, 496, and 156, for the boxes of size of 1. 2, 4, 8, and 16, respectively. Therefore, the vector [5619, 3028, 1436, 496, 156] are assumed as a global image feature for this brain image.

C. RESULT OF OUR METHOD

The accuracy results of our proposed method (PSO-TTC) over three datasets are 100%, 98.19%, and 98.08%, respectively. We list the detailed result over each run and each fold in Table 2 and Table 3. In the tables, $a(b)$ represents a brain images were successfully recognized among b brain images.

D. COMPARISON TO OPTIMIZATION METHODS

In the fourth experiment, we compared the proposed PSO-TTC with standard genetic algorithm (GA), particle swarm optimization (PSO), artificial bee colony (ABC), and firefly algorithm (FA). Their parameters were obtained by trial and error method. The results are listed in Table 4.

TABLE 2. Accuracy of our method over D_2.

	F1	F2	F3	F4	F5	Total	Acc. (%)
R1	32(32)	32(32)	32(32)	31(32)	31(32)	158(160)	98.75
R2	32(32)	32(32)	32(32)	31(32)	32(32)	159(160)	99.38
R3	31(32)	29(32)	31(32)	31(32)	32(32)	154(160)	96.25
R4	30(32)	31(32)	31(32)	31(32)	32(32)	155(160)	96.88
R5	32(32)	31(32)	32(32)	30(32)	32(32)	157(160)	98.13
R6	32(32)	31(32)	32(32)	32(32)	31(32)	158(160)	98.75
R7	32(32)	31(32)	32(32)	32(32)	31(32)	158(160)	98.75
R8	32(32)	31(32)	30(32)	32(32)	32(32)	157(160)	98.13
R9	32(32)	32(32)	32(32)	31(32)	32(32)	159(160)	99.38
R10	31(32)	31(32)	32(32)	31(32)	31(32)	156(160)	97.50
Total							98.19

The accuracies in Table 4 show that the GA achieves 96.52%, 89.31%, and 88.78% for the three datasets, respectively. PSO achieves 98.33%, 96.56%, and 96.20%, respectively. ABC achieves 97.73%, 93.94%, and 92.75%, respectively. FA achieves 97.42%, 94.50%, and 94.04%, respectively. Our proposed method achieves the best accuracy as 100.00%, 98.19%, and 98.08%.

Why the PSO-TTC performs better than other four global optimization methods? The reasons are apparent:

TABLE 3. Accuracy of our method over D_3.

	F1	F2	F3	F4	F5	Total	Acc. (%)
R1	49(51)	51(51)	50(51)	49(51)	50(51)	249(255)	97.65
R2	49(51)	50(51)	51(51)	49(51)	50(51)	249(255)	97.65
R3	51(51)	51(51)	51(51)	50(51)	49(51)	252(255)	98.82
R4	51(51)	51(51)	49(51)	51(51)	51(51)	253(255)	99.22
R5	50(51)	50(51)	51(51)	49(51)	49(51)	249(255)	97.65
R6	51(51)	50(51)	50(51)	50(51)	50(51)	251(255)	98.43
R7	51(51)	51(51)	50(51)	50(51)	51(51)	253(255)	99.22
R8	50(51)	50(51)	49(51)	50(51)	50(51)	249(255)	97.65
R9	51(51)	49(51)	50(51)	50(51)	49(51)	249(255)	97.65
R10	48(51)	49(51)	50(51)	50(51)	50(51)	247(255)	96.86
Total							98.08

TABLE 4. PSO-TTC versus state-of-the-art optimization methods.

Method	D_1	D_2	D_3
GA	96.52	89.31	88.78
PSO	98.33	96.56	96.20
ABC	97.73	93.94	92.75
FA	97.42	94.50	94.04
PSO-TTC (Proposed)	**100.00**	**98.19**	**98.08**

(Bold means the best)

(1) The proposed three-segment particle representation (TSPR) encode not only the weights and biases, but also the number of hidden neurons. Hence, PSO-TTC has the unique ability to optimize the number of hidden neurons. (2) We embed the time-varying acceleration coefficient (TVAC), which enhances the global search ability in the initial stage, and augment the local search ability in the end stage. (3) The logistical map in chaos theory brings more versatility into the particle swarm. Those three methods guarantee the effectiveness of our method.

E. COMPARISON TO STATE-OF-THE-ART APPROACHES

In the fifth experiment, we compared WPTE + FNN + RCBBO, with 11 state-of-the-art approaches. Table 5 showed the comparison results based on five or ten runs of SCV.

The comparison results in Table 5 demonstrated that this proposed "MBD+SLFN+PSO-TTC" yields the best detection accuracy among all approaches. It even gives perfect detection over the D_1 dataset. This indicates the artificial intelligence makes a progress in this PBDS, and our developed PBDS is better result than 11 state-of-the-art methods. Another advantage of our method is that we used the least of features with number of 5, which indicates our extracted features are efficient than others.

F. COMPUTATION TIME

In the finale, we run ten times and record the average computation time (ACT) in training and prediction stages. The hardware platform is Dell desktop with 3.20 GHz Intel i5-3470 CPU and 4GB RAM. The software platform is 64bit Win10 Operating System and Matlab R2015a.

Table 6 shows that the ACT over D_3 dataset cost 53.41 seconds on MBD calculation, and the ACT of MBD calculation over one brain image only costs 0.1960 second. The reason is the D_3 contains 255 images. Next, the training of SLFN using PSO-TTC costs 32.11 seconds, while output of a trained SLFN only uses 0.0024 seconds. This result suggests our method may be time-consuming in training, but it is rather quick in prediction. For one-image prediction, it only costs 0.1984 seconds.

TABLE 5. Classification comparison (Bold means the best).

Existing approaches	Feature No.	Run No.	D_1	D_2	D_3
DWT+SOM [56]	4761	5	94.00	93.17	91.65
DWT + SVM + RBF [56]	4761	5	98.00	97.33	96.18
DWT + PCA + ANN [57]	7	5	97.00	96.98	95.29
DWT + PCA + KNN [57]	7	5	98.00	97.54	96.79
DWT + PCA + SVM [58]	19	5	96.01	95.00	94.29
WE + NBC [59]	7	10	92.58	91.87	90.51
WN + SVM [60]	7	10	82.58	80.13	77.76
WPSE + SVM [61]	16	10	98.64	97.12	97.02
FRFE + WTT + NBC [62]	12	10	97.12	95.94	95.69
FRFE + MLP + BBO [63]	12	10	99.09	97.81	95.76
FRFE + MLP + RCBBO [63]	12	10	99.24	97.69	96.12
MBD + SLFN + PSO-TTC (Proposed)	5	10	**100.00**	**98.19**	**98.08**

(DWT = discrete wavelet transform; SOM = self-organization map; SVM = support vector machine; PCA = principal component analysis; ANN = artificial neural network; kNN = k nearest neighbors; WE = wavelet entropy; NBC = naive Bayes classifier; WN = wavelet energy; WPSE = wavelet packet Shannon entropy; FRFE = fractional Fourier entropy; MLP = multilayer perceptron; BBO = biogeography-based optimization; RCBBO = real-coded BBO; MBD = Minkowski-Bouligand dimension; SLFN = single layer feedforward neural-network; PSO = particle swarm optimization)

TABLE 6. Computation time (Unit: Second).

Training over D_3	ACT
MBD	53.41
SLFN + PSO-TTC	32.11
Prediction over one image	**ACT**
MBD	0.1960
Trained SLFN	0.0024

(ACT = average computation time)

VIII. CONCLUSIONS

In this study, we proposed a novel PBDS for detecting abnormal MR brain images. The experiments showed our method was superior to 11 state-of-the-art PBDSs.

The main contribution lies in the use of fractal dimension that is an important branch of fractional calculus, which is a new field studying the possibility of taking real number powers or complex numbers of the differential operator and the integration operator [64]. We believe fractional calculus will be applied into brain science extensively, since the fractional operators can describe the brain structures in both macro-level and micro-level.

In the future, we will begin following tentative medical-related researches: (i) Brain segmentation [65] will be included, and the MBD will be extracted from gray matter, white matter, and cerebrospinal fluid regions, respectively.

(ii) Try other advanced learning models, such as extreme learning machine [66]. (ii) Apply our method to CT images [67] and PET images [68].

We shall test computing-related techniques: (i) Test other advanced optimization methods, such as biogeography-based optimization [69]. (ii) Wearable computing [70] based on wireless body area network [71] or wireless sensor network [72] can help detect abnormal brains in real time. (iii) Recommendation system [73] can be used to suggest treatment. (iv) New computer science related techniques, such as cloud computing [74], internet of things [75], and big data [76] will be included.

We shall try to extend our method to following mathematical-related areas: (i) Extend our method to volumetric image and apply fractal dimension on 3D surfaces [77]. (ii) The fractional calculus [78] will be tested on extract new features.

CONFLICT OF INTEREST

We have no conflicts of interest to disclose with regard to the subject matter of this paper.

REFERENCES

[1] R. Sutter and P. W. Kaplan, "What to see when you are looking at confusion: A review of the neuroimaging of acute encephalopathy," *J. Neurol. Neurosurgery Psychiatry*, vol. 86, no. 4, pp. 446–459, Apr. 2015.

[2] S. Arslan, N. Poyraz, R. Ucar, M. Yesildag, A. Yesildag, and A. Z. Caliskaner, "Magnetic resonance imaging may be a valuable radiation-free technique for lung pathologies in patients with primary immunodeficiency," *J. Clin. Immunol.*, vol. 36, no. 1, pp. 66–72, Jan. 2016.

[3] G. Caiazzo, F. Trojsi, M. Cirillo, G. Tedeschi, and F. Esposito, "Q-ball imaging models: Comparison between high and low angular resolution diffusion-weighted MRI protocols for investigation of brain white matter integrity," *Neuroradiology*, vol. 58, no. 2, pp. 209–215, Feb. 2016.

[4] Y. Zhang, "Detection of alzheimer's disease by displacement field and machine learning," *PeerJ*, vol. 3, Sep. 2015, Art. no. e1251.

[5] P. Phillips, Z. Dong, G. Ji, and J. Yang, "Detection of alzheimer's disease and mild cognitive impairment based on structural volumetric MR images using 3D-DWT and WTA-KSVM trained by PSOTVAC," *Biomed. Signal Process. Control*, vol. 21, pp. 58–73, Aug. 2015.

[6] T. Hachaj and M. R. Ogiela, "Application of neural networks in detection of abnormal brain perfusion regions," *Neurocomputing*, vol. 122, pp. 33–42, Dec. 2013.

[7] E. S. A. El-Dahshan, H. M. Mohsen, K. Revett, and A. B. M. Salem, "Computer-aided diagnosis of human brain tumor through MRI: A survey and a new algorithm," *Expert Syst. Appl.*, vol. 41, no. 11, pp. 5526–5545, Sep. 2014.

[8] S. Wang *et al.*, "Feed-forward neural network optimized by hybridization of PSO and ABC for abnormal brain detection," *Int. J. Imag. Syst. Technol.*, vol. 25, no. 2, pp. 153–164, 2015.

[9] Y. Zhang, S. Wang, P. Sun, and P. Phillips, "Pathological brain detection based on wavelet entropy and Hu moment invariants," *BioMed. Mater. Eng.*, vol. 26, no. 1, pp. 1283–1290, 2015.

[10] A. Wibmer *et al.*, "Haralick texture analysis of prostate MRI: Utility for differentiating non-cancerous prostate from prostate cancer and differentiating prostate cancers with different Gleason scores," *Eur. Radiol.*, vol. 25, no. 10, pp. 2840–2850, Oct. 2015.

[11] Z. Dong, G. Ji, J. Yang, Y. Zhang, and S. Wang, "Preclinical diagnosis of magnetic resonance (MR) brain images via discrete wavelet packet transform with Tsallis entropy and generalized eigenvalue proximal support vector machine (GEPSVM)," *Entropy*, vol. 17, no. 4, pp. 1795–1813, 2015.

[12] Z. Dong, A. Liu, S. Wang, G. Ji, Z. Zhang, and J. Yang, "Magnetic resonance brain image classification via stationary wavelet transform and generalized eigenvalue proximal support vector machine," *J. Med. Imag. Health Inf.*, vol. 5, pp. 1395–1403, Dec. 2015.

[13] V. Rajagopalan *et al.*, "Brain white matter shape changes in amyotrophic lateral sclerosis (ALS): A fractal dimension study," *PloS ONE*, vol. 8, Sep. 2013, Art. no. e73614.

[14] S. Farahibozorg, S. M. Hashemi-Golpayegani, and J. Ashburner, "Age- and sex-related variations in the brain white matter fractal dimension throughout adulthood: An MRI study," *Clin. Neuroradiol.*, vol. 25, pp. 19–32, Mar. 2015.

[15] S. Z. Mirjalili, S. Saremi, and S. M. Mirjalili, "Designing evolutionary feedforward neural networks using social spider optimization algorithm," *Neural Comput. Appl.*, vol. 26, no. 8, pp. 1919–1928, Nov. 2015.

[16] S. Gholizadeh, "Performance-based optimum seismic design of steel structures by a modified firefly algorithm and a new neural network," *Adv. Eng. Softw.*, vol. 81, pp. 50–65, Mar. 2015.

[17] S. Lahmiri, "Interest rate next-day variation prediction based on hybrid feedforward neural network, particle swarm optimization, and multiresolution techniques," *Phys. A, Statistical Mech. Appl.*, vol. 444, pp. 388–396, Feb. 2016.

[18] S. Das, M. Chowdhury, and M. K. Kundu, "Brain MR image classification using multiscale geometric analysis of ripplet," *Progr. Electromagn. Res. Pier*, vol. 137, pp. 1–17, May 2013.

[19] S. Purushotham and B. K. Tripathy, "Evaluation of classifier models using stratified tenfold cross validation techniques," in *Global Trends in Information Systems and Software Applications*, vol. 270, P. V. Krishna, M. R. Babu, and E. Ariwa, Eds. Berlin, Germany: Springer-Verlag, 2012, pp. 680–690.

[20] M. Salmasi, U. Büttner, and S. Glasauer, "Fractal dimension analysis for spike detection in low SNR extracellular signals," *J. Neural Eng.*, vol. 13, no. 3, Jun. 2016, Article ID: 036004.

[21] N. Macé, A. Jagannathan, and F. Piéchon, "Fractal dimensions of wave functions and local spectral measures on the fibonacci chain," *Phys. Rev. B*, vol. 93, May 2016, Article ID: 205153.

[22] S. Yadav, R. Choudhary, U. Soni, B. Peswani, and M. M. Sharma, "Koch curve fractal antenna for wi-MAX and C-Band wireless applications," in *Proc. Int. Conf. Confluence Next Generat. Inf. Technol.* Summit, Amity Univ., Noida, IN, Sep. 2014, pp. 490–494.

[23] S. Lahmiri and M. Boukadoum, "Automatic brain MR images diagnosis based on edge fractal dimension and spectral energy signature," in *Proc. Annu. Int. Conf. IEEE Eng. Med. Biol. Soc.*, New York, NY, USA, Sep. 2012, pp. 6243–6246.

[24] J. X. Du, C. M. Zhai, and Q. P. Wang, "Recognition of plant leaf image based on fractal dimension features," *Neurocomputing*, vol. 116, pp. 150–156, Sep. 2013.

[25] A. Yarlagadda, J. V. R. Murthy, and M. Prasad, "A comparative study of fractal dimension based age group classification of facial images with different testing strategies," in *3rd Int. Conf. Frontiers Intell. Comput. Theory Appl.*, Bhubaneswar, India, 2015, pp. 229–240.

[26] D. Amarasinghe, U. Sonnadara, M. Berg, and V. Cooray, "Fractal dimension of long electrical discharges," *J. Electrostatics*, vol. 73, pp. 33–37, Feb. 2015.

[27] H. Zhong *et al.*, "Edge detection and fractal dimension analysis of CT images to predict outcome of rectal cancer with neoadjuvant chemoradiation," *Int. J. Radiation Oncol. Biol. Phys.*, vol. 93, p. S182, Nov. 2015.

[28] D. C. Costa, C. A. B. Mello, and T. J. dos Santos, "Boundary detection based on chromatic color difference and morphological texture suppression," in *Proc. Int. Conf. Syst.*, Manchester, England, 2013, pp. 4305–4310.

[29] Y. He, R. Fu, L. Y. Liu, and Y. Q. Zhang, "An image edge thinning algorithm based on fuzzy classifications," in *Proc. Int. Conf. Adv. Mech. Eng. Ind. Informat.*, Zhengzhou, China, 2015, pp. 219–223.

[30] A. R. Imre and J. Bogaert, "The Minkowski-Bouligand dimension and the interior-to-edge ratio of habitats," *Fractals-Complex Geometry Patterns Scaling Nature Soc.*, vol. 14, pp. 49–53, Mar. 2006.

[31] M. Luppe, "Fractal dimension based on minkowski-bouligand method using exponential dilations," *Electron. Lett.*, vol. 51, no. 6, pp. 475–476, Mar. 2015.

[32] M. Bouda, J. S. Caplan, and J. E. Saiers, "Box-counting dimension revisited: Presenting an efficient method of minimizing quantization error and an assessment of the self-similarity of structural root systems," *Frontiers plant Sci.*, vol. 7, Feb. 2016, Art. no. 149.

[33] S. K. Sharma and P. Chandra, "A constructive algorithm with adaptive sigmoidal function for designing single hidden layer feedforward neural network," in *Mems, Nano And Smart Systems*, vols. 403–408, L. Yuan, Ed. Stäfa, Switzerland: Trans Tech Publications Ltd, 2012, pp. 3867–3874.

[34] Y. Zhang, S. Wang, P. Phillips, and G. Ji, "Fruit classification using computer vision and feedforward neural network," *J. Food Eng.*, vol. 143, pp. 167–177, Dec. 2014.
[35] L. K. Li, S. Shao, and K. F. C. Yiu, "A new optimization algorithm for single hidden layer feedforward neural networks," *Appl. Soft Comput.*, vol. 13, no. 5, pp. 2857–2862, May 2013.
[36] L. Hu, L. H. Qin, K. Mao, W. Y. Chen, and X. Fu, "Optimization of neural network by genetic algorithm for flowrate determination in multipath ultrasonic gas flowmeter," *IEEE Sensors J.*, vol. 16, no. 3, pp. 1158–1167, Mar. 2016.
[37] F. Han and J. S. Zhu, "Improved Particle Swarm Optimization Combined with backpropagation for feedforward neural networks," *Int. J. Intell. Syst.*, vol. 28, pp. 271–288, Mar. 2013.
[38] Y. M. M. Hassim and R. Ghazali, "Using artificial bee colony to improve functional link neural network training," in *Information Technology Applications in Industry*, vols. 263–266, J. Zhang, Z. J. Wang, S. R. Zhu, and X. M. Meng, Eds. ed Stäfa, Switzerland: Trans Tech Publications Ltd., 2013, pp. 2102–2108.
[39] G. Yang *et al.*, "Automated classification of brain images using wavelet-energy and biogeography-based optimization," *Multimedia Tools Appl.*, May 2015, doi: 10.1007/s11042-015-2649-7.
[40] Y. Zhang, G. Ji, and S. Wang "A comprehensive survey on particle swarm optimization algorithm and its applications," *Math. Problems Eng.*, Feb. 2015, Art. no. 931256.
[41] F. Shahzad, S. Masood, and N. K. Khan, "Probabilistic opposition-based particle swarm optimization with velocity clamping," *Knowl. Inf.Systems*, vol. 39, pp. 703–737, Jun. 2014.
[42] S. Banerjee, K. Dasgupta, and C. K. Chanda, " Cover image short term hydroŰwindŰthermal scheduling based on particle swarm optimization technique," *Int. J. Electr. Power Energy Syst.*, vol. 81, pp. 275–288, Oct. 2016.
[43] J. T. Bryson, X. Jin, and S. K. Agrawal, "Optimal design of cable-driven manipulators using particle swarm optimization," *J. Mech. Robot Trans. ASME*, vol. 8, Aug. 2016, Art. no. 041003.
[44] G. Ji, Y. Zhang, P. Phillip, Z. Dong, and J. Yang, "Pathological brain detection in magnetic resonance imaging scanning by wavelet entropy and hybridization of biogeography-based optimization and particle swarm optimization," *Prog. Electromagn. Res.*, vol. 152, pp. 41–58, Sep. 2015.
[45] M. Manbachi, H. Farhangi, A. Palizban, and S. Arzanpour, "Smart grid adaptive energy conservation and optimization engine utilizing Particle Swarm Optimization and Fuzzification," *Appl. Energy*, vol. 174, pp. 69–79, Jul. 2016.
[46] P. Bhatia, K. K. Mishra, D. Kumar, and A. Kumar, "An improved-time varying acceleration coefficient based PSO," *J. Multiple-Valued Logic Soft Comput.*, vol. 26, nos. 3–5, pp. 189–204, 2016.
[47] S. H. Wang, P. Phillips, J. F. Yang, P. Sun, and Y. D. Zhang, "Magnetic resonance brain classification by a novel binary particle swarm optimization with mutation and time-varying acceleration coefficients," *Biomed. Eng.-Biomedizinische Tech.*, vol. 61, pp. 431–441, Aug. 2016.
[48] R. Solanki, K. T. Chaturvedi, and N. P. Patidar, "Different penalty handling based economic dispatch using time varying acceleration coefficients," in *Proc. Swarm, Evol., Memetic Comput.*, Bhubaneswar, India, 2015, pp. 750–764.
[49] F. Denis and C. Letellier, "Radiotherapy and chaos theory: The tit and the butterfly," *Cancer Radiotherapie*, vol. 16, pp. 404–409, Sep. 2012.
[50] Y. Zhang and L. Wu, "Crop classification by forward neural network with adaptive chaotic particle swarm optimization," *Sensors*, vol. 11, no. 5, pp. 4721–4743, 2011.
[51] Y. Zhang, Y. Jun, G. Wei, and L. Wu, "Find multi-objective paths in stochastic networks via chaotic immune PSO," *Expert Syst. Appl.*, vol. 37, no. 3, pp. 1911–1919, 2010.
[52] A. Jain and N. Rajpal, "A robust image encryption algorithm resistant to attacks using DNA and chaotic logistic maps," *Multimedia Tools Appl.*, vol. 75, pp. 5455–5472, May 2016.
[53] H. B. Di and D. L. Gao, "Gray-level transformation and Canny edge detection for 3D seismic discontinuity enhancement," *Comput. Geosciences*, vol. 72, pp. 192–200, Nov. 2014.
[54] S. Singh and A. Datar, "Improved hash based approach for secure color image steganography using canny edge detection method," *Int. J. Comput. Sci. Netw. Security*, vol. 15, pp. 92–98, Jul. 2015.
[55] J. Yasmin and M. Sathik, "An improved iterative segmentation algorithm using canny edge detector for skin lesion border detection," *Int. Arab J. Inf. Technol.*, vol. 12, pp. 325–332, Jul. 2015.
[56] L. M. Patnaik, S. Chaplot, and N. R. Jagannathan, "Classification of magnetic resonance brain images using wavelets as input to support vector machine and neural network," *Biomed. Signal Process. Control*, vol. 1, no. 1,pp. 86–92, 2006.
[57] E. S. A. El-Dahshan, T. Hosny, and A. B. M. Salem, "Hybrid intelligent techniques for MRI brain images classification," *Digit. Signal Process.*, vol. 20, pp. 433–441, Mar. 2010.
[58] B. Y. Zhang and L. Wu, "An MR brain images classifier via principal component analysis and kernel support vector machine," *Prog. Electromagn. Res.*, vol. 130, pp. 369–388, Oct. 2012.
[59] X. Zhou *et al.*, "Detection of pathological brain in MRI scanning based on wavelet-entropy and naive Bayes classifier," in *Bioinformatics and Biomedical Engineering*, vol. 9043, F. Ortuño and I. Rojas, Eds. Granada, Spain: Springer, 2015, pp. 201–209.
[60] Z. Guang-Shuai *et al.*, "Automated Classification of Brain MR Images using Wavelet-Energy and Support Vector Machines," in *Proc. Int. Conf. Mechatron., Electron., Ind. Control Eng.*, C. Liu, G. Chang, and Z. Luo, Eds., USA: Atlantis Press, 2015, pp. 683–686.
[61] G. Liu *et al.*, "Pathological brain detection in MRI scanning by wavelet packet Tsallis entropy and fuzzy support vector machine," *SpringerPlus*, vol. 4, Nov. 2015, Art. no. 716.
[62] X. Yang, P. Sun, Z. Dong, A. Liu, and T.-F. Yuan, "Pathological brain detection by a novel image feature—Fractional Fourier entropy," *Entropy*, vol. 17, no. 12, pp. 8278–8296, 2015.
[63] Y. Zhang, P. Phillips, G. Liu, S. Wang, X. Zhou, and Y. Sun, "A multilayer perceptron based smart pathological brain detection system by fractional Fourier entropy," *J. Med. Syst.*, vol. 40, no. 7, 2016, Art. no. 173.
[64] X.-J. Wang, J. A. Tenreiro Machado, D. Baleanu, and C. Cattani, "On exact traveling-wave solutions for local fractional Korteweg-de Vries equation," *Chaos*, vol. 26, no. 8, p. 084312, 2016.
[65] M. Havaei, H. Larochelle, P. Poulin, and P. M. Jodoin, "Within-brain classification for brain tumor segmentation," *Int. J. Of Comput. Assist. Radiol. Surgery*, vol. 11, pp. 777–788, May 2016.
[66] S. Lu, Z. Lu, J. Yang, M. Yang, and S. Wang. (2016). A pathological brain detection system based on kernel based ELM, *Multimedia Tools Appl.* pp. 1–14, 2016, doi: 10.1007/s11042-016-3559-z.
[67] Y. Chen *et al.*, "Curve-like structure extraction using minimal path propagation with backtracking," *IEEE Trans. Image Process.*, vol. 25, no. 2, pp. 988–1003, Feb. 2016.
[68] H. Tsukada, M. Kanazawa, H. Ohba, S. Nishiyama, N. Harada, and T. Kakiuchi, "PET imaging of mitochondrial complex I with 18F-BCPP-EF in the brains of MPTP-treated monkeys.," *J. Of Nucl. Med.*, vol. 57, pp. 950–953, Jun. 2016.
[69] S. Wang, Y. Zhang, G. Ji, J. Yang, J. Wu, and L. Wei, "Fruit classification by wavelet-entropy and feedforward neural network trained by fitness-scaled chaotic ABC and biogeography-based optimization," *Entropy*, vol. 17, no. 8, pp. 5711–5728, 2015.
[70] M. Chen, Y. Zhang, Y. Li, M. M. Hassan, and A. Alamri, "AIWAC: Affective interaction through wearable computing and cloud technology," *IEEE Wireless Commun.*, vol. 22, no. 1, pp. 20–27, Feb. 2015.
[71] L. Hu, Y. Zhang, D. Feng, M. M. Hassan, A. Alelaiwi, and A. Alamri, "Design of QoS-Aware multi-level MAC-layer for wireless body area network," *J. Med. Syst.*, vol. 39, no. 12, Dec. 2015, Art. no. 192.
[72] J. Wang, Y. Zhang, Z. Cheng, and X. Zhu, "EMIP: Energy-efficient itinerary planning for multiple mobile agents in wireless sensor network," *Telecommun. Syst.*, vol. 62, no. 1, pp. 93–100, May 2016.
[73] Y. Zhang, "GroRec: A group-centric intelligent recommender system integrating social, mobile and big data technologies," *IEEE Trans. Serv. Comput.*, Jan. 2016, doi: 10.1109/TSC.2016.2592520.
[74] Y. Ma, Y. Zhang, J. Wan, D. Zhang, and N. Pan, "Robot and cloud-assisted multi-modal healthcare system," *Cluster Comput. J. Netw. Softw. Tools Appl.*, vol. 18, pp. 1295–1306, Sep. 2015.
[75] Y. Ma, Y. Zhang, O.-M. Dung, R. Li, and D. Zhang, "Health Internet of Things: Recent applications and outlook," *J. Internet Technol.*, vol. 16, pp. 351–362, Mar. 2015.
[76] Y. Zhang, M. Chen, S. W. Mao, L. Hu, and V. Leung, "CAP: Community activity prediction based on big data analysis," *IEEE Netw.*, vol. 28, no. 4, pp. 52–57, Jul./Aug. 2014.
[77] A. Laaksonen, J. Malila, A. Nenes, H. M. Hung, and J. P. Chen, "Surface fractal dimension, water adsorption efficiency, and cloud nucleation activity of insoluble aerosol," *Sci. Rep.*, vol. 6, May 2016, Art. no. 25504.

[78] X. J. Yang and H. M. Srivastava, "An asymptotic perturbation solution for a linear oscillator of free damped vibrations in fractal medium described by local fractional derivatives," *Commun. Nonlinear Sci. Numer. Simul.*, vol. 29, pp. 499–504, Dec. 2015.

YU-DONG ZHANG received the Ph.D. degree in signal and information processing from Southeast University in 2010. From 2010 to 2012, he held a post-doctoral position with Columbia University. From 2012 to 2013, he was an Assistant Research Scientist with Columbia University. He is currently a Full Professor and a Doctoral Advisor with the School of Computer Science and Technology, Nanjing Normal University. His research interests focus on computer-aided diagnosis and biomedical image processing.

XIAN-QING CHEN received the Ph.D. degree in information and communication engineering from Southeast University, China, in 2013. He is currently an Associate Professor with the Department of Electrical Engineering, College of Engineering, Zhejiang Normal University. His research interest is image processing and information theory.

TIAN-MING ZHAN received the Ph.D. degree in pattern recognition and intelligence system from the Nanjing University of Science and Technology, Nanjing, China, in 2013. He is currently an Associate Professor with the School of Technology, Nanjing Audit University. His research interests include in medical imaging processing and analysis.

ZHU-QING JIAO received the Ph.D. degree in control theory and control engineering from Jiangnan University, Wuxi, China, in 2011. He is currently an Associate Professor with the School of Information Science and Engineering, Changzhou University. His research interests include in complex networks computing and brain information processing.

YI SUN received the Ph.D. degree from the State Key Laboratory of Networking and Switching Technology, Beijing University of Posts and Telecommunications in 2015. She is currently a Lecturer with the Institute of Sensing Technology and Business, Beijing University of Posts and Communications, China. Her research interests include information security, privacy-preserving data mining, secure multiparty computation, and healthcare big data.

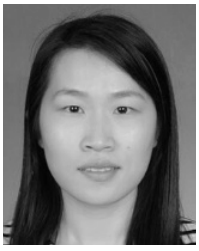

ZHI-MIN CHEN received the M.S. degree from the Shandong University of Technology in 2010, and the Ph.D. degree from Southeast University in 2015. She is currently with Shanghai Dianji University. Her research interest is in the areas of information and communication theory.

YU YAO was born in 1986. He received the Ph.D. degree in electrical engineering from Southeast University, China, in 2015. He is currently a Lecturer with the Huadong Jiaotong University. His research focuses on the communication and radar signal processing, and cognitive radio.

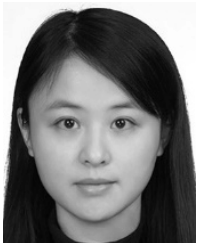

LAN-TING FANG received the M.S. degree from Ninbo University in 2013. She is currently pursuing the Ph.D. degree with the School of Information Science and Engineering, Southeast University. Her research interest is natural language processing and machine learning.

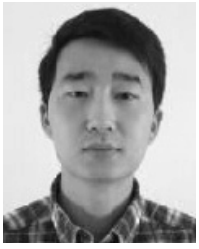

YI-DING LV received the degree from the Qiqihar Medical College in 2014. He is currently pursuing the master's degree with the Department of Psychiatry, Nanjing Medical University.

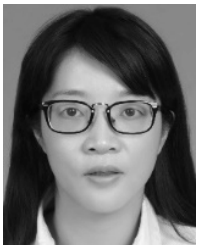

SHUI-HUA WANG received the B.S. degree from Southeast University in 2008, the M.S. degree from The City University of New York in 2012, and the Ph.D. degree from Nanjing University in 2016. She is currently an Assistant Professor with Nanjing Normal University.